Automated Reconstruction of 3D Open Surfaces from Sparse Point Clouds

Mohammad Samiul Arshad*
The University of Texas at Arlington

William J. Beksi†
The University of Texas at Arlington
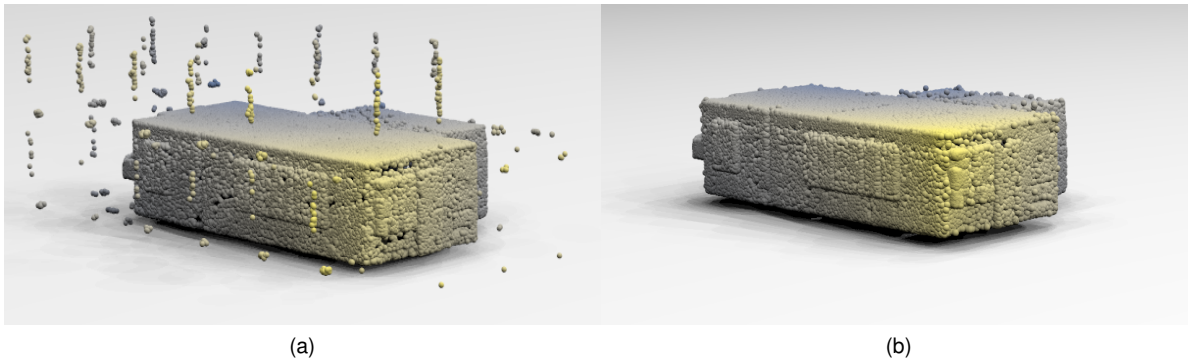
Figure 1: An outside view of a dense 3D reconstructed scene from the Gibson Environment [50] dataset using (a) NDF [15], and (b) our proposed approach. Note that our method produces significantly less outliers.

ABSTRACT

Real-world 3D data may contain intricate details defined by salient surface gaps. Automated reconstruction of these open surfaces (*e.g.*, non-watertight meshes) is a challenging problem for environment synthesis in mixed reality applications. Current learning-based implicit techniques can achieve high fidelity on closed-surface reconstruction. However, their dependence on the distinction between the *inside* and *outside* of a surface makes them incapable of reconstructing open surfaces. Recently, a new class of implicit functions have shown promise in reconstructing open surfaces by regressing an unsigned distance field. Yet, these methods rely on a *discretized representation* of the raw data, which loses important surface details and can lead to outliers in the reconstruction. We propose IPVNet, a learning-based implicit model that predicts the unsigned distance between a surface and a query point in 3D space by leveraging both raw point cloud data and its discretized voxel counterpart. Experiments on synthetic and real-world public datasets demonstrates that IPVNet *outperforms* the state of the art while producing *far fewer* outliers in the reconstruction.

Index Terms: Automated/semi-automated reconstruction—Open-surface reconstruction—Unsigned distance field

1 INTRODUCTION

Capturing detailed point cloud data from the real world is a difficult and expensive task. Moreover, due to the limitations of 3D sensor technologies (*e.g.*, LiDAR, RGB-D, etc.), data can be sparse (*i.e.*, missing details) and incomplete (*i.e.*, noisy with holes and outliers) [19, 26]. Automated reconstruction of the missing parts and the reintroduction of surface details is not a trivial task. Researchers have looked into a myriad of ways [1–3,9,10,17,20,21,24,25,31,36, 40,44,52] to complete 3D data. Recently, learning-based implicit

---
*e-mail: mohammadsamiul.arshad@mavs.uta.edu
†e-mail: william.beksi@uta.edu

functions [8, 12, 14, 15, 18, 32, 37] have become popular among 3D reconstruction techniques due to their ability to generate data in arbitrary resolutions.

One set of implicit learning techniques [4, 5] makes use of raw point cloud data to learn a signed distance field. Since traditional convolutions cannot be applied on permutation invariant point clouds, such methods often depend on linear feature aggregation through a multilayer perceptron [39] or they define a dynamic kernel and perform a neighborhood search to mimic convolutions [45]. Other implicit methods [14, 15] discretize the raw point clouds into voxel grids. However, voxel grids lose information since multiple points within the boundary of a grid are merged together. Moreover, the computational costs and memory requirements increase *cubically* using this approach. Implicit functions that learn an SDF via extraction of a zero level set must distinguish between the inside and outside of the surface. As a result, the reconstruction is produced as a closed surface even if the target shape includes surface gaps [5]. However, real-world point cloud data can consist of salient open surfaces. Closing the surface of such data often leads to the introduction of outliers and lost details.

To reconstruct accurate geometry and preserve surface details, we propose IPVNet, an implicit model that learns a unsigned distance field (UDF) by accumulating features from raw point clouds and voxel grids jointly to reconstruct open surfaces. As shown in Fig. 1, our approach produces significantly less outliers compared to the state of art [15]. To the best of our knowledge, our work is the first approach on combining point-voxel features to learn implicit functions. Our key contributions can be summarized as follows.

- We introduce IPVNet, a novel approach for implicitly learning from raw point cloud and voxel features to automatically reconstruct complex open surfaces.

- We develop an inference module that extracts a zero level set from a UDF and drastically lowers the amount of outliers in the reconstruction.

- We show that IPVNet outperforms the state-of-the art on both synthetic and real-world public datasets.

2 RELATED WORK

3D reconstruction is a well researched area with a number of different approaches and algorithms [1–3, 9, 10, 17, 20, 21, 24, 25, 31, 36, 40, 44, 52]. In this section, we review and compare our work with learning-based implicit approaches. For a more comprehensive review, we refer to contemporary surveys on 3D reconstruction [6, 53].

2.1 Implicit Function Learning

Instead of explicitly predicting a surface, implicit feature learning methods try to either predict if a particular point in 3D space is inside or outside of a target surface (occupancy), or determine how far the point is from the target surface (distance). To reconstruct 3D data in arbitrary resolutions and learn a continuous 3D mapping, Mescheder *et al.* [32] presented a network that predicts voxel occupancy. Peng *et al.* [38] improved the occupancy network by incorporating 2D and 3D convolutions. An encoder-decoder architecture was used by Chen *et al.* [12] to learn voxel occupancy. Michalkiewicz *et al.* [33] estimates oriented level set to extract 3D surface. Littwin and Wolf [29] used encoded feature vectors as the network weights to predict voxel occupancy. Park *et al.* [37] introduced DeepSDF, an encoder-decoder based architecture that predicts a signed distance to the surface instead of voxel occupancy. Genova *et al.* [18] divided an object's surface into a set of shape elements and used an encoder-decoder to learn occupancy. Chibane *et al.* [14] used 3D feature tensors to predict voxel occupancy. Rather than transforming point clouds into a occupancy grid, Atzmon and Lipman used the raw point clouds to learn and predict an SDF to the target surface in [4], and incorporated derivatives in regression loss to further improve the reconstruction accuracy in [5].

All of the aforementioned works either predict a voxel occupancy or signed distance value for a given query point, which is inadequate to reconstruct open surfaces. To address this problem, we task IPVNet to learn an unsigned distance field. Prior to our work, Chibane *et al.* [15] predicted a UDF from an input voxel occupancy map. A similar technique to learn a UDF for single-view garment reconstruction was used by Zhao *et al.* [55]. Venkatesh *et al.* [47] proposed a closest surface point representation to reconstruct both open and close surfaces. However, preceding work on UDFs often discretize the raw point cloud data into voxel grids, which results in lost surface details. In contrast, we make use of the raw point cloud *jointly* with voxel occupancy, thus enabling us to accumulate improved features and reconstruct finer details with less outliers.

2.2 Learning from Points and Voxels

Recently, fusion between features extracted from point cloud and voxel representations has shown to improve the performance of 3D computer vision methods. Liu *et al.* [30] introduced PVCNN to perform classification and segmentation by extracting features from both point clouds and voxel grids via voxelization and de-voxelization. Fusion between voxel and point features for 3D classification was used by Li *et al.* [27]. Shi *et al.* [41] gathered multi-scale voxel features which were combined into keypoint features from a point cloud for object detection and further improved the results by incorporating local vector pooling in [42]. Using PVCNN as a backbone, Zhu *et al.* [56] performed shape completion and generation through point-voxel diffusion. Point-voxel fusion to detect 3D objects was used by Cui *et al.* [16] and Tang *et al.* [43] learned a 3D model via sparse point-voxel convolution.

Noh *et al.* [35] accumulated point-voxel features in a single representation for 3D object detection. PVT, a transformer-based architecture that learns from point-voxel features for point cloud segmentation was introduced by Zhang *et al.* [54]. Wei *et al.* [48] used point-voxel correlation for scene flow estimation and Li *et al.* [28] used point-voxel convolution for 3D object detection. Xu *et al.* [51] introduced RPVNet for point cloud segmentation via point-voxel fusion. Cherenkova *et al.* [13] utilized point-voxel deconvolution
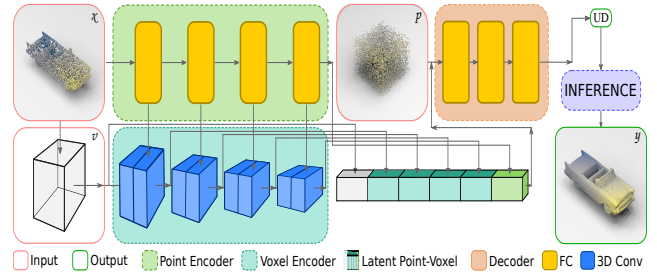
Figure 2: Given a sparse point cloud $x \in \mathcal{X}$ of an object, we use a novel encoding scheme to extract and aggregate point-voxel features from both the raw point cloud (x) and the voxel occupancy (v). From the accumulated features, a decoder module regresses the unsigned distance $UD(p, S)$ from query point p to the surface S. By querying the decoder multiple times, the inference sub-module can reconstruct the surface of any target shape.

for point cloud encoding/decoding. In contrast to the preceding research, we focus on applying point-voxel fusion to the task of learning implicit functions and open-surface reconstruction. To the best of our knowledge, our approach is the first attempt to understand the effectiveness of point-voxel fusion on these tasks.

3 IMPLICIT LEARNING WITH POINT-VOXEL FEATURES

An overview of our network is presented in Fig. 2. Given a sparse point cloud $x \in \mathcal{X} \subset \mathbb{R}^{N \times 3}$ of an object, we use a novel encoding scheme to extract and aggregate point-voxel features from both the raw point cloud (x) and the voxel occupancy (v). From the accumulated features, a decoder module regresses the unsigned distance $UD(p, S)$ from any query point p to the surface S. In the following subsections we describe the elements of our approach.

3.1 Point-Voxel Features

To extract a set of multilevel features from a point cloud x, we define a neural function

$$\Theta(x) := (z_x^1, \ldots, z_x^j) \,|\, \Theta \colon \mathbb{R}^{N \times 3} \to \mathbb{Z}, \tag{1}$$

where $z_x \in \mathbb{Z} \subset \mathbb{R}$ corresponds to the extracted feature vector from the raw point cloud x, and j is the total number of layers in Θ. ReLu [34] non-linearity is used for all layers except the output layer of the point encoder.

Instead of limiting the encoded features to a single dimensional vector, a voxel representation allows for the construction of a multidimensional latent matrix. However, such an encoding scheme requires the input point cloud x to be discretized into a voxel grid v, *i.e.*, $x \approx v \colon \mathbb{R}^{N \times 3} \to \mathbb{R}^{M \times M \times M}$ where $M \in \mathbb{N}$ is the grid resolution. Due to the discretization process, voxel grids lose information since multiple points may lie within the same voxel. To reintroduce lost details, we combine voxel features with point features z_x.

Let $\Phi \colon \mathbb{R}^{M \times M \times M} \to \mathbb{Z}^{M \times M \times M}$ be a neural function that encodes the combined point-voxel features into a set of multidimensional feature grid z_{xv} of monotonically decreasing dimension. Then,

$$\Phi(v \odot \Theta(x)) := (z_{xv}^{k \times k \times k}, \ldots, z_{xv}^{l \times l \times l}), \tag{2}$$

where $k, l \in \mathbb{N}$ represents the dimensional upper and lower bound of the feature grid ($M > k \gg l > 1$), the subscript xv denotes the dependency on both points and voxels. Similar to its point counterpart, the voxel encoder is more directed towards local details at the early stages. However, as the dimensionality is reduced and the receptive field grows larger, the aim shifts to the global structure. ReLu is utilized to ensure non-linearity and batch normalization [22] provides stability while training. The latent point (z_x^j) from the point

encoder, along with multidimensional features (z_{xv}) from the point-voxel encoder and the discretized voxel grid (v), are then used to construct the latent point-voxel

$$z = \{z_x^j, \Phi(v \odot \Theta(x)), v\}. \quad (3)$$

3.2 Implicit Decoding

Given a query point $p \in \mathbb{R}^3$, a set of deep features F_p is sampled from the latent point-voxel features z via a spatial grid sampling [23] function Ω. Specifically,

$$\Omega(z, p) := (F_p^1 \times \cdots \times F_p^n), \quad (4)$$

where $n = |z|$. Similar to [14], we extract features from a neighborhood of distance $d \in \mathbb{R}$ along the Cartesian axes centered at p to obtain rich features. More formally,

$$p := \{p + q \cdot c_i \cdot d\} \in \mathbb{R}^3 \mid q \in \{1, 0, -1\}, i \in \{1, 2, 3\}, \quad (5)$$

where $c_i \in \mathbb{R}^3$ is the ith Cartesian axis unit vector. We define a neural function Ψ that regresses the unsigned distance to the surface S of x from the deep features (F_p). Concretely,

$$\Psi(F_p^1, \ldots, F_p^n) \cong UD(p, S) \mid \Psi : \mathbb{Z} \to \mathbb{R}_+, \quad (6)$$

where $UD(\cdot)$ is a function that returns the unsigned distance from p to the ground-truth surface S for any $p \in \mathbb{R}^3$. Therefore, the implicit decoder to regress the unsigned distance at a given query point p is defined as

$$f_x(z, p) := (\Omega \circ \Psi)(p) \mid f_x : \mathbb{Z} \times \mathbb{R}^3 \to \mathbb{R}_+. \quad (7)$$

3.3 Training

IPVNet requires a pair $\{X_i, S_i\}_{i=1}^T$ associated with input X_i and corresponding ground-truth surface S_i for implicit learning. Parameterized by the neural parameter w, the point-encoder, voxel-encoder, and decoder are jointly trained with a mini-batch loss

$$\mathsf{L_B} := \Sigma_{x \in B} \Sigma_{p \in \mathsf{P}} |\min(f_x^w(p), \delta) - \min(UD(p, S_x), \delta)|, \quad (8)$$

where B is a mini-batch of input and $\mathsf{P} \in \mathbb{R}^{Q \times 3}$ is a set of query points within distance δ of S_i. Similar to [15], we use a clamped distance $0 < \delta < 10$ (cm) to improve the models capacity to represent the vicinity of the surface accurately.

3.4 Surface Inference

Analogous to [15], we use an iterative strategy to extract surface points from f_x. More specifically, given a perfect approximator $f_x(p)$ of the true unsigned distance $UD(p, S_i)$, the projection of p onto the surface S_i can be obtained by

$$q := p - f_x(p) \cdot \nabla_p f_x(p), q \in S_i \subset \mathbb{R}^d, \forall p \in \mathbb{R}^d / C. \quad (9)$$

In (9), C is the cut locus [49], *i.e.*, a set of points that are equidistant to at least two surface points. The negative gradient indicates the direction of the fastest decrease in distance. In addition, we can move a distance of $f_x(p)$ to reach q if the norm of the gradient is one. By projecting a point multiple times via (9), the inaccuracies due to $f_x(p)$ being an imperfect approximator can be reduced. Furthermore, filtering the projected points to a maximum distance threshold (*max_thresh*) and re-projecting them onto the surface after displacement by $d \sim \mathcal{N}(0, \delta/3)$ can ensure higher point density within a maximum distance (δ).

Instead of uniformly sampling query points within the bounding box of S_i [15], we use the input points $X_i \in \mathbb{R}^3$ as guidance for the query points. In particular, we apply a random uniform jitter $J_a^b \in \mathbb{R}^3$ within bounds a and b to displace the input points X_i. Due to the inclusion of point features in learning, this procedure allows our model to infer more accurate surface points while restricting the number of outliers. The details of the inference procedure are provided in Alg. 1.

Algorithm 1 Surface Point Inference

1: **procedure** INFERENCE(X)
2:     $np \leftarrow$ Total number of projections
3:     $T \leftarrow$ Maximum threshold distance
4:     $R \leftarrow$ Output resolution of the point cloud
5:     $\mathsf{J} \leftarrow m$ points from $\mathcal{U}(a, b)$
6:     $\mathsf{P}_{init} \leftarrow \{x + j\}, \forall x \in \mathsf{X}, \forall j \in \mathsf{J}$
7:     **for** $i = 1$ to np **do**
8:         $p \leftarrow p - f_x(p) \cdot \frac{\nabla_p f_x(p)}{\|\nabla_p f_x(p)\|}, \forall p \in \mathsf{P}_{init}$
9:     **end for**
10:    $\mathsf{P}_{filtered} \leftarrow \{p \in \mathsf{P}_{init} \mid f_x(p) < T\}$
11:    $\mathsf{P}_{filtered}$: draw R points with replacement
12:    $\mathsf{P}_{filtered} \leftarrow \{p + d\} \mid p \in \mathsf{P}_{filtered}, d \sim \mathcal{N}(0, \delta/3)$
13:    **for** $i = 1$ to np **do**
14:        $p \leftarrow p - f_x(p) \cdot \frac{\nabla_p f_x(p)}{\|\nabla_p f_x(p)\|}, \forall p \in \mathsf{P}_{filtered}$
15:    **end for**
16:    **return** $\{p \in \mathsf{P}_{filtered} \mid f_x(p) < T\}$
17: **end procedure**

4 EXPERIMENTS

To validate the performance of IPVNet we concentrate on the task of 3D object and scene reconstruction from sparse point clouds. In this section, we present the details of the experimental setup and provide an analysis of our results.
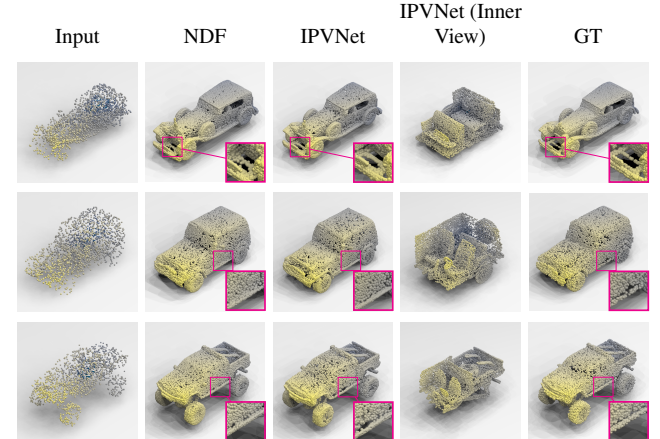
Figure 3: Object reconstruction using NDF [15], IPVNet, and the ground truth (GT) from the ShapeNet Cars [11] test set. IPVNet performs better on reconstructing thin structures and preserving small gaps (inset images).

4.1 Baseline and Metric

We utilize a neural distance field (NDF) [15] as the baseline to compare the reconstruction quality of IPVNet. To the best of our knowledge, NDF [15] and CSP [47] are the only approaches available for open surface reconstruction. However, due to the unavailability of the codebase for multi-shape learning via CSP, we compare our results only against NDF. Note that, to be fair, we do not compare against methods that are limited to closed surface reconstruction as our main objective is the reconstruction of open surfaces. For an unbiased comparison, we trained an NDF following the directions from [15] on our train-test split until a minimum validation accuracy was achieved.

To quantitatively measure the reconstruction quality, we use the *chamfer-L_2* distance (CD) to measure the accuracy and completeness of the surface. The CD is defined as

$$d_{CD}(Y, Y_{gt}) = \sum_{i \in Y} \min_{j \in Y_{gt}} ||i - j||^2 + \sum_{j \in Y_{gt}} \min_{i \in Y} ||j - i||^2, \quad (10)$$

where $Y_{gt} \in \mathbb{R}^{\mathcal{O} \times 3}$ is the ground-truth point cloud, $Y \in \mathbb{R}^{\mathcal{O} \times 3}$ is the reconstructed point cloud, and $\mathcal{O} \in \mathbb{N}$ is the point density of the ground truth and the output. In addition, precision and recall are two metrics that have been extensively used to evaluate 3D reconstruction results. Precision quantifies the accuracy while recall assesses the completeness of the reconstruction. For the ground truth Y_{gt} and reconstructed point cloud Y, the precision of an outcome at a threshold d can be calculated as

$$P(d) = \sum_{i \in Y} [\min_{j \in Y_{gt}} ||i - j|| < d].$$

Similarly, the recall for a given d may be computed as

$$R(d) = \sum_{j \in Y_{gt}} [\min_{i \in Y} ||j - i|| < d].$$

The F-score, proposed in [46] as a comprehensive evaluation, combines precision and recall to quantify the overall reconstruction quality. In detail, the F-score at d is given by

$$F(d) = \frac{2 \cdot P(d) \cdot R(d)}{P(d) + R(d)}.$$

An F-score of 1 indicates perfect reconstruction.

4.2 Object Reconstruction

Due to the abundance of surface openings, we have chosen the "Cars" subset from the ShapeNet [11] dataset for our object reconstruction experiment. We used a random split of 70%-10%-20% for training, validation, and testing, respectively. To prepare the ground truth and input points we followed the data preparation procedure outlined in [15]. Additionally, we fixed the output point density $\mathcal{O} = 1$ million to extract a smooth mesh from the point cloud using a naive algorithm (*e.g.*, [7]).

To understand the effects of sparse input on the reconstruction quality, we evaluated IPVNet and the baseline using an input density of $N \sim \{300, 3000, 10000\}$ points while fixing the voxel resolution to $M = 256$. In contrast to the baseline, IPVNet can reconstruct thin structures more accurately and preserve small gaps (see the inset images in Fig. 3) while quantitatively outperforming the reconstruction with different input densities (Table 1).

	Chamfer-L_2 ↓			F-score ↑	
	$N = 300$	$N = 3000$	$N = 10000$	$d = 0.1\%$	$d = 0.05\%$
NDF	1.550	0.324	0.092	0.711	0.460
IPVNet	**1.217**	**0.119**	**0.068**	**0.785**	**0.542**

Table 1: A quantitative comparison between IPVNet and the baseline (NDF [15]) on the ShapeNet Cars [11] dataset for object reconstruction from different input densities. IPVNet outperforms the baseline on all input densities. The chamfer-L_2 results are of order $\times 10^{-4}$ and the reconstruction results using an input density of $N = 10000$ were used to calculate the *F-score*.

4.3 Real-World Scene Reconstruction

We evaluate the reconstruction of complex real-world scenes through the use of the Gibson Environment dataset [50]. The dataset consists of RDG-D scans of indoor spaces. A subset of 35 and 100 scenes were prepared following the procedure from [15] for training and testing respectively. We used a sliding window scheme and reconstructed the surface bounded by each window. Since the sliding window may frequently consist of a very small area of the scene with only few points, we used an output density five times as large the input density (*i.e.*, $\mathcal{O} = 5 \times N$) to save time. The grid resolutions were kept fixed at $M = 256$ for both IPVNet and the baseline. The reconstruction results are highlighted in Fig. 4. In addition to improving the preservation of structural details, IPVNet produces significantly fewer outliers than the baseline due to the use of point features during training and inference.
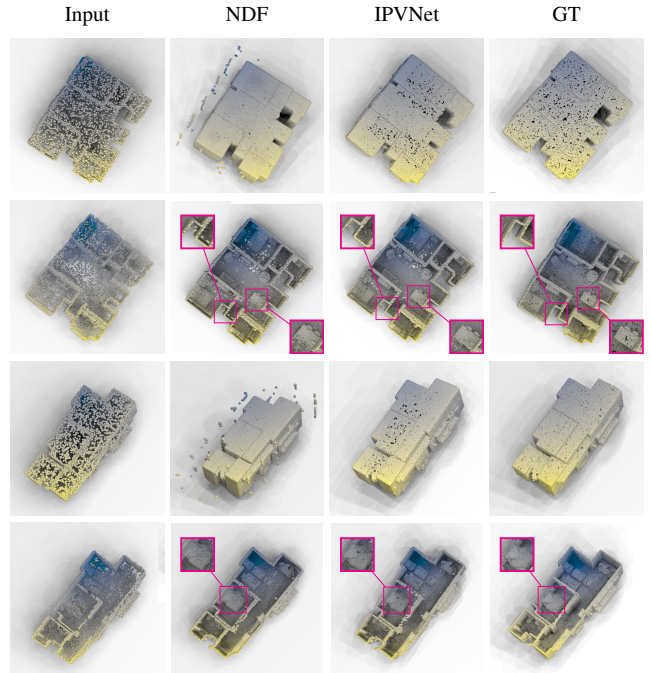
Figure 4: Scene reconstruction on the test set of the Gibson Environment [50] dataset using NDF [15], IPVNet, and the respective ground truth (GT). Each odd row represents an outside view of a scene while the even rows depict inside views. In contrast to the baseline, IPVNet produces significantly less outliers (outside view) and improves the preservation of geometric features (inset images).

5 CONCLUSION

In this work we have introduced IPVNet, a novel architecture for automatically reconstructing complex open surfaces. To do this, we make use of raw point cloud data jointly with voxels to learn local and global features. Not only have we showed that IPVNet outperforms the state of the art on both synthetic and real-world data, but we also demonstrated the effectiveness of point features on 3D reconstruction through ablation studies. Furthermore, we developed an inference module that extracts a zero level set from a UDF and drastically reduces the amount of outliers in the reconstruction. IPVNet is an important step towards reconstructing open surfaces without losing details and introducing outliers. We believe that our work will inspire more research on this topic.

REFERENCES

[1] N. Amenta, M. Bern, and M. Kamvysselis. A new voronoi-based surface reconstruction algorithm. In *Proceedings of the Conference on Computer Graphics and Interactive Techniques*, pp. 415–421, 1998.

[2] N. Amenta, S. Choi, T. K. Dey, and N. Leekha. A simple algorithm for homeomorphic surface reconstruction. In *Proceedings of the Symposium on Computational Geometry*, pp. 213–222, 2000.

[3] N. Amenta, S. Choi, and R. K. Kolluri. The power crust. In *Proceedings of the ACM Symposium on Solid Modeling and Applications*, pp. 249–266, 2001.

[4] M. Atzmon and Y. Lipman. Sal: Sign agnostic learning of shapes from raw data. In *Proceedings of the IEEE/CVF Conference on Computer Vision and Pattern Recognition*, pp. 2565–2574, 2020.

[5] M. Atzmon and Y. Lipman. Sald: Sign agnostic learning with derivatives. *arXiv preprint arXiv:2006.05400*, 2020.

[6] M. Berger, A. Tagliasacchi, L. M. Seversky, P. Alliez, G. Guennebaud, J. A. Levine, A. Sharf, and C. T. Silva. A survey of surface reconstruction from point clouds. *Computer Graphics Forum*, 36(1):301–329, 2017.

[7] F. Bernardini, J. Mittleman, H. Rushmeier, C. Silva, and G. Taubin. The ball-pivoting algorithm for surface reconstruction. *IEEE Transactions on Visualization and Computer Graphics*, 5(4):349–359, 1999.

[8] B. L. Bhatnagar, C. Sminchisescu, C. Theobalt, and G. Pons-Moll. Combining implicit function learning and parametric models for 3d human reconstruction. In *Proceedings of the European Conference on Computer Vision*, pp. 311–329. Springer, 2020.

[9] F. Calakli and G. Taubin. Ssd: Smooth signed distance surface reconstruction. *Computer Graphics Forum*, 30(7):1993–2002, 2011.

[10] J. C. Carr, R. K. Beatson, J. B. Cherrie, T. J. Mitchell, W. R. Fright, B. C. McCallum, and T. R. Evans. Reconstruction and representation of 3d objects with radial basis functions. In *Proceedings of the Conference on Computer Graphics and Interactive Techniques*, pp. 67–76, 2001.

[11] A. X. Chang, T. Funkhouser, L. Guibas, P. Hanrahan, Q. Huang, Z. Li, S. Savarese, M. Savva, S. Song, H. Su, et al. Shapenet: An information-rich 3d model repository. *arXiv preprint arXiv:1512.03012*, 2015.

[12] Z. Chen and H. Zhang. Learning implicit fields for generative shape modeling. In *Proceedings of the IEEE/CVF Conference on Computer Vision and Pattern Recognition*, pp. 5939–5948, 2019.

[13] K. Cherenkova, D. Aouada, and G. Gusev. Pvdeconv: Point-voxel deconvolution for autoencoding cad construction in 3d. In *Proceedings of the IEEE International Conference on Image Processing*, pp. 2741–2745, 2020.

[14] J. Chibane, T. Alldieck, and G. Pons-Moll. Implicit functions in feature space for 3d shape reconstruction and completion. In *Proceedings of the IEEE/CVF Conference on Computer Vision and Pattern Recognition*, pp. 6970–6981, 2020.

[15] J. Chibane, A. Mir, and G. Pons-Moll. Neural unsigned distance fields for implicit function learning. *arXiv preprint arXiv:2010.13938*, 2020.

[16] Z. Cui and Z. Zhang. Pvf-net: Point & voxel fusion 3d object detection framework for point cloud. In *Proceedings of the Conference on Computer and Robot Vision*, pp. 125–133. IEEE, 2020.

[17] A. Gálvez, A. Cobo, J. Puig-Pey, and A. Iglesias. Particle swarm optimization for bézier surface reconstruction. In *Proceedings of the International Conference on Computational Science*, pp. 116–125. Springer, 2008.

[18] K. Genova, F. Cole, A. Sud, A. Sarna, and T. Funkhouser. Local deep implicit functions for 3d shape. In *Proceedings of the IEEE/CVF Conference on Computer Vision and Pattern Recognition*, pp. 4857–4866, 2020.

[19] P. Guerrero, Y. Kleiman, M. Ovsjanikov, and N. J. Mitra. Pcpnet learning local shape properties from raw point clouds. *Computer Graphics Forum*, 37(2):75–85, 2018.

[20] H. Hoppe, T. DeRose, T. Duchamp, J. McDonald, and W. Stuetzle. Surface reconstruction from unorganized points. In *Proceedings of the Conference on Computer Graphics and Interactive Techniques*, pp. 71–78, 1992.

[21] H. Huang, D. Li, H. Zhang, U. Ascher, and D. Cohen-Or. Consolidation of unorganized point clouds for surface reconstruction. *ACM Transactions on Graphics*, 28(5):1–7, 2009.

[22] S. Ioffe and C. Szegedy. Batch normalization: Accelerating deep network training by reducing internal covariate shift. In *Proceedings of the International Conference on Machine Learning*, pp. 448–456, 2015.

[23] M. Jaderberg, K. Simonyan, A. Zisserman, et al. Spatial transformer networks. In *Proceedings of the Advances in Neural Information Processing Systems*, vol. 28, 2015.

[24] M. Kazhdan, M. Bolitho, and H. Hoppe. Poisson surface reconstruction. In *Proceedings of the Eurographics Symposium on Geometry Processing*, vol. 7, 2006.

[25] M. Kazhdan and H. Hoppe. Screened poisson surface reconstruction. *ACM Transactions on Graphics*, 32(3):1–13, 2013.

[26] R. Li, X. Li, C.-W. Fu, D. Cohen-Or, and P.-A. Heng. Pu-gan: A point cloud upsampling adversarial network. In *Proceedings of the IEEE/CVF International Conference on Computer Vision*, pp. 7203–7212, 2019.

[27] Y. Li, G. Tong, X. Li, L. Zhang, and H. Peng. Mvf-cnn: Fusion of multilevel features for large-scale point cloud classification. *IEEE Access*, 7:46522–46537, 2019.

[28] Y. Li, S. Yang, Y. Zheng, and H. Lu. Improved point-voxel region convolutional neural network: 3d object detectors for autonomous driving. *IEEE Transactions on Intelligent Transportation Systems*, 2021.

[29] G. Littwin and L. Wolf. Deep meta functionals for shape representation. In *Proceedings of the IEEE/CVF International Conference on Computer Vision*, pp. 1824–1833, 2019.

[30] Z. Liu, H. Tang, Y. Lin, and S. Han. Point-voxel cnn for efficient 3d deep learning. *arXiv preprint arXiv:1907.03739*, 2019.

[31] J. Manson, G. Petrova, and S. Schaefer. Streaming surface reconstruction using wavelets. *Computer Graphics Forum*, 27(5):1411–1420, 2008.

[32] L. Mescheder, M. Oechsle, M. Niemeyer, S. Nowozin, and A. Geiger. Occupancy networks: Learning 3d reconstruction in function space. In *Proceedings of the IEEE/CVF Conference on Computer Vision and Pattern Recognition*, pp. 4460–4470, 2019.

[33] M. Michalkiewicz, J. K. Pontes, D. Jack, M. Baktashmotlagh, and A. Eriksson. Deep level sets: Implicit surface representations for 3d shape inference. *arXiv preprint arXiv:1901.06802*, 2019.

[34] V. Nair and G. E. Hinton. Rectified linear units improve restricted boltzmann machines. In *Proceedings of the International Conference on Machine Learning*, 2010.

[35] J. Noh, S. Lee, and B. Ham. Hvpr: Hybrid voxel-point representation for single-stage 3d object detection. In *Proceedings of the IEEE/CVF Conference on Computer Vision and Pattern Recognition*, pp. 14605–14614, 2021.

[36] Y. Ohtake, A. Belyaev, M. Alexa, G. Turk, and H.-P. Seidel. Multi-level partition of unity implicits. In *ACM SIGGRAPH 2005 Courses*, pp. 173–es. 2005.

[37] J. J. Park, P. Florence, J. Straub, R. Newcombe, and S. Lovegrove. Deepsdf: Learning continuous signed distance functions for shape representation. In *Proceedings of the IEEE/CVF Conference on Computer Vision and Pattern Recognition*, pp. 165–174, 2019.

[38] S. Peng, M. Niemeyer, L. Mescheder, M. Pollefeys, and A. Geiger. Convolutional occupancy networks. In *Proceedings of the European Conference on Computer Vision*, pp. 523–540. Springer, 2020.

[39] C. R. Qi, H. Su, K. Mo, and L. J. Guibas. Pointnet: Deep learning on point sets for 3d classification and segmentation. In *Proceedings of the IEEE/CVF Conference on Computer Vision and Pattern Recognition*, pp. 652–660, 2017.

[40] X. Ren, L. Lyu, X. He, W. Cao, Z. Yang, B. Sheng, Y. Zhang, and E. Wu. Biorthogonal wavelet surface reconstruction using partial integrations. *Computer Graphics Forum*, 37(7):13–24, 2018.

[41] S. Shi, C. Guo, L. Jiang, Z. Wang, J. Shi, X. Wang, and H. Li. Pv-rcnn: Point-voxel feature set abstraction for 3d object detection. In *Proceedings of the IEEE/CVF Conference on Computer Vision and Pattern Recognition*, pp. 10529–10538, 2020.

[42] S. Shi, L. Jiang, J. Deng, Z. Wang, C. Guo, J. Shi, X. Wang, and H. Li. Pv-rcnn++: Point-voxel feature set abstraction with local vector representation for 3d object detection. *arXiv preprint arXiv:2102.00463*, 2021.

[43] H. Tang, Z. Liu, S. Zhao, Y. Lin, J. Lin, H. Wang, and S. Han. Searching efficient 3d architectures with sparse point-voxel convolution. In *Proceedings of the European Conference on Computer Vision*, pp. 685–702. Springer, 2020.

[44] Y. Tang and J. Feng. Multi-scale surface reconstruction based on a curvature-adaptive signed distance field. *Computers & Graphics*, 70:28–38, 2018.

[45] M. Tatarchenko, A. Dosovitskiy, and T. Brox. Octree generating networks: Efficient convolutional architectures for high-resolution 3d outputs. In *Proceedings of the IEEE/CVF International Conference on Computer Vision*, pp. 2088–2096, 2017.

[46] M. Tatarchenko, S. R. Richter, R. Ranftl, Z. Li, V. Koltun, and T. Brox. What do single-view 3d reconstruction networks learn? In *Proceedings of the IEEE/CVF Conference on Computer Vision and Pattern Recognition*, pp. 3405–3414, 2019.

[47] R. Venkatesh, T. Karmali, S. Sharma, A. Ghosh, R. V. Babu, L. A. Jeni, and M. Singh. Deep implicit surface point prediction networks. In *Proceedings of the IEEE/CVF International Conference on Computer Vision*, pp. 12653–12662, 2021.

[48] Y. Wei, Z. Wang, Y. Rao, J. Lu, and J. Zhou. Pv-raft: point-voxel correlation fields for scene flow estimation of point clouds. In *Proceedings of the IEEE/CVF Conference on Computer Vision and Pattern Recognition*, pp. 6954–6963, 2021.

[49] F.-E. Wolter. Cut locus and medial axis in global shape interrogation and representation, design laboratory memorandum 92-2, 1993.

[50] F. Xia, A. R. Zamir, Z. He, A. Sax, J. Malik, and S. Savarese. Gibson env: Real-world perception for embodied agents. In *Proceedings of the IEEE/CVF Conference on Computer Vision and Pattern Recognition*, pp. 9068–9079, 2018.

[51] J. Xu, R. Zhang, J. Dou, Y. Zhu, J. Sun, and S. Pu. Rpvnet: A deep and efficient range-point-voxel fusion network for lidar point cloud segmentation. In *Proceedings of the IEEE/CVF International Conference on Computer Vision*, pp. 16024–16033, 2021.

[52] J. Yang, Z. Wang, C. Zhu, and Q. Peng. Implicit surface reconstruction with radial basis functions. In *Proceedings of the International Conference on Computer Vision and Computer Graphics*, pp. 5–12. Springer, 2007.

[53] C. C. You, S. P. Lim, S. C. Lim, J. San Tan, C. K. Lee, and Y. M. J. Khaw. A survey on surface reconstruction techniques for structured and unstructured data. In *Proceedings of the IEEE Conference on Open Systems*, pp. 37–42, 2020.

[54] C. Zhang, H. Wan, S. Liu, X. Shen, and Z. Wu. Pvt: Point-voxel transformer for 3d deep learning. *arXiv preprint arXiv:2108.06076*, 2021.

[55] F. Zhao, W. Wang, S. Liao, and L. Shao. Learning anchored unsigned distance functions with gradient direction alignment for single-view garment reconstruction. In *Proceedings of the IEEE/CVF International Conference on Computer Vision*, pp. 12674–12683, 2021.

[56] Q. Zhu, L. Chen, Q. Li, M. Li, A. Nüchter, and J. Wang. 3d lidar point cloud based intersection recognition for autonomous driving. In *Proceedings of the IEEE Intelligent Vehicles Symposium*, pp. 456–461, 2012.